HHS Public Access

Author manuscript

Biomaterials. Author manuscript; available in PMC 2022 June 01.

Published in final edited form as:

Biomaterials. 2021 June ; 273: 120810. doi:10.1016/j.biomaterials.2021.120810.

miR-145 Micelles Mitigate Atherosclerosis by Modulating Vascular Smooth Muscle Cell Phenotype

Deborah D. Chin[a,‡], **Christopher Poon**[a,‡,1], **Jonathan Wang**[a], **Johan Joo**[a], **Victor Ong**[a], **Zhangjingyi Jiang**[a], **Kayley Cheng**[a], **Anastasia Plotkin**[b], **Gregory A. Magee**[b], **Eun Ji Chung**[*,a,b,c,d,e,f]

[a]Department of Biomedical Engineering, University of Southern California, Los Angeles, CA, 90089, United States

[b]Division of Vascular Surgery and Endovascular Therapy, Department of Surgery, Keck School of Medicine, University of Southern California, Los Angeles, CA, 90033, United States

[c]Mork Family Department of Chemical Engineering and Materials Science, University of Southern California, Los Angeles, CA, 90089, United States

[d]Eli and Edythe Broad Center for Regenerative Medicine and Stem Cell Research, Keck School of Medicine, University of Southern California, Los Angeles, CA, 90033, United States

[e]Division of Nephrology and Hypertension, Department of Medicine, Keck School of Medicine, University of Southern California, Los Angeles, CA, 90033, United States

[f]Norris Comprehensive Cancer Center, Keck School of Medicine, University of Southern California, Los Angeles, CA, 90089, United States

Abstract

[*]Corresponding author: Eun Ji Chung, Department of Biomedical Engineering, University of Southern California, 1042 Downey Way, DRB 140, Los Angeles, CA 90089, Tel.: +1-213-740-2825, Fax: +1-213-821-3897, eunchung@usc.edu.

‡These authors contributed equally to this work.

[1]Present Address: Christopher Poon, Emergent Biosolutions, 3985-A Sorrento Valley Blvd, San Diego, CA 92121

Author contributions

The manuscript was written through contributions of all authors. All authors have given approval to the final version of the manuscript. ‡These authors contributed equally. E.J.C. conceived the project and E.J.C., D.C. and C.P. designed the experiments; C.P., D.C., J.W., J.J., V.O., Z.J., K.C., and E.J.C. performed the experiments and analyzed the data; C.P., D.C, and E.J.C wrote the manuscript. All authors have read and approved the final manuscript.

Deborah Chin and Christopher Poon contributed equally. Eun Ji Chung.: Conceptualization, Methodology, Validation, Visualization, Writing, Supervision. Deborah Chin: Methodology, Validation, Investigation, Visualization, Writing. Christopher Poon: Methodology, Investigation, Validation, Visualization, Writing. Jonathan Wang: Investigation. Johan Joo: Investigation. Victor Ong: Investigation. Kayley Cheng: Investigation. Zhangjingyi Jiang: Investigation. All authors have read and approved the final manuscript.

Competing interests

There are no competing interests to state.

Declaration of interests

The authors declare that they have no known competing financial interests or personal relationships that could have appeared to influence the work reported in this paper.

Data Availability

The raw/processed data required to reproduce these findings cannot be shared at this time due to technical or time limitations.

In atherosclerosis, resident vascular smooth muscle cells (VSMCs) in the blood vessels become highly plastic and undergo phenotypic switching from the quiescent, contractile phenotype to the migratory and proliferative, synthetic phenotype. Additionally, recent VSMC lineage-tracing mouse models of atherosclerosis have found that VSMCs transdifferentiate into macrophage-like and osteochondrogenic cells and make up to 70% of cells found in atherosclerotic plaques. Given VSMC phenotypic switching is regulated by microRNA-145 (miR-145), we hypothesized that nanoparticle-mediated delivery of miR-145 to VSMCs has the potential to mitigate atherosclerosis development by inhibiting plaque-propagating cell types derived from VSMCs. To test our hypothesis, we synthesized miR-145 micelles targeting the C-C chemokine receptor-2 (CCR2), which is highly expressed on synthetic VSMCs. When miR-145 micelles were incubated with human aortic VSMCs *in vitro*, >90% miR-145 micelles escaped the lysosomal pathway in 4 hours and released the miR cargo under cytosolic levels of glutathione, an endogenous reducing agent. As such, miR-145 micelles rescued atheroprotective contractile markers, myocardin, α-SMA, and calponin, in synthetic VSMCs *in vitro*. In early-stage atherosclerotic ApoE$^{-/-}$ mice, one dose of miR-145 micelles prevented lesion growth by 49% and sustained an increased level of miR-145 expression after 2 weeks post-treatment. Additionally, miR-145 micelles inhibited 35% and 43% plaque growth compared to free miR-145 and PBS, respectively, in mid-stage atherosclerotic ApoE$^{-/-}$ mice. Collectively, we present a novel therapeutic strategy and cell target for atherosclerosis, and present miR-145 micelles as a viable nanotherapeutic that can intervene atherosclerosis progression at both early and later stages of disease.

Keywords

Peptide; Micelle; Nanomedicine; microRNA; Atherosclerosis; Smooth muscle cell

Introduction

Vascular smooth muscle cells (VSMCs) are the predominant cell type in blood vessel walls and are responsible for maintaining vessel wall integrity, elasticity, and contractility [1]. In healthy vessels, VSMCs maintain a quiescent, contractile phenotype, but in response to injury or aging, such as atherosclerosis, VSMCs lose their contractile markers and dedifferentiate into an overproliferative and migratory synthetic phenotype and transdifferentiate into inflammatory macrophages and calcifying osteochondrogenic cells that can propagate disease [2, 3]. Recent *in vivo* VSMC lineage-tracing studies in atherosclerotic mice have elucidated that 30–70% of the cell population in atherosclerotic plaques are originally derived from VSMCs and hence, interventions that can modulate VSMC phenotype and transdifferentiation may serve as a “multi-target” therapy in atherosclerosis by inhibiting multiple, plaque-propagating cell types [4, 5].

MicroRNAs (miRs) are short, non-coding, 22–24 nucleotide RNAs that demonstrate post-transcriptional gene silencing capabilities [6]. In particular, miR-145 is the most highly expressed miR in the vasculature and maintains the VSMC contractile phenotype by promoting contractile genes, myocardin, calponin, and alpha-smooth muscle actin (α-SMA), while downregulating synthetic genes, Krüppel-like factor-4/5 (KLF-4/5) and ETS domain-containing protein-1 (ELK-1) [7, 8]. Clinically, patients with atherosclerosis have reduced

levels of circulating miR-145 and regions of vascular damage express little to undetectable levels of miR-145 [7, 9, 10]. Thus, we hypothesize that delivery of miR-145 to VSMCs has the potential to mitigate plaque development by promoting the contractile VSMC phenotype.

Delivering nucleic acids *in vivo*, however, has challenges including degradation by nucleases, which limits drug half-life in circulation, and dilution in off-target tissues, which can lead to adverse side effects [11–13]. To overcome these limitations and improve the delivery of nucleic acids, we previously reported on the development of peptide amphiphile micelle (PAM) nanoparticles that can be specifically delivered to pathological features in atherosclerosis such as monocytes and microthrombi, and reported on their *in vivo* stability, biocompatibility, and potential for drug delivery [14–16]. Given the growing knowledge and significance of VSMCs in atherosclerosis in recent years, in this study, we designed a novel strategy using PAMs to mitigate VSMC phenotypic modulation through miR-145 delivery.

Specifically, we developed PAMs consisting of the targeting moiety, monocyte chemoattractant protein-1 (MCP-1) peptide, for delivery of miR-145 to atherosclerotic lesions (miR-145 micelles). MCP-1/C-C motif chemokine ligand 2 (CCL2) is the high affinity ligand for C-C chemokine receptor-2 (CCR2), a receptor that is highly expressed on synthetic VSMCs. Additionally, CCR2 has been reported to be expressed on monocytes and macrophages that make up atherosclerotic plaques [17]. Thus, the use of MCP-1 for facilitated delivery of miR-145 is an attractive strategy to increase local concentration of miR-145 in plaques. To evaluate the efficacy of miR-145 micelles, we tested the ability of miR-145 micelles to bind to VSMCs and inhibit phenotypic switching *in vitro* using patient-derived VSMCs, and evaluated their ability to mitigate atherosclerosis at early- and mid-stage disease in the ApoE knock-out ($ApoE^{-/-}$) mouse model. Additionally, we evaluated the pharmacokinetic properties, safety, and toxicity of this novel nanotherapeutic. Together, we report the therapeutic potency of miR-145 micelles and its potential application during multiple stages of atherosclerosis.

Materials and Methods

General Experimental.

All starting materials were purchased from Sigma-Aldrich (St. Louis, MO) and Fisher Scientific (Waltham, MA), unless otherwise noted. hASMCs (ATCC# PCS-100–012, Manassas, VA) were purchased from ATCC and subjected to mycoplasma testing. hASMCs were cultured in Medium 231 (Thermo Fisher Scientific, Waltham, MA), supplemented with smooth muscle growth supplement (SMGS, Thermo Fisher Scientific, Waltham, MA) and 1% penicillin-streptomycin (Thermo Fisher Scientific, Waltham, MA). The use of human tissues in this study was approved by the Institutional Biosafety Committee (IBC #BUA-16–00057) and Institutional Review Board (IRB #HS-18–00638, BUA-18–0031) at the University of Southern California. Informed consent was obtained from patients for collection of tissue discarded during the normal course of their operation. Segments of the right pulmonary artery and aorta without plaque and samples from the posterior tibial artery with severe atherosclerosis were collected from male patients. Tissue samples were stored in Hank’s balanced salt solution (HBSS) for no longer than 16 hours prior to VSMC harvest and cell culture.

The VSMC harvest and cell culture procedure was adapted from previous reports [18]. Briefly, tissue samples were washed and rinsed three times with HBSS before the endothelium and adventitia were removed, the medial layer sectioned into 1–2 mm^2 explants, and digested with 0.25% collagenase type II and 0.5% elastase type II for 16 hours at 37°C. The explant solution was centrifuged at 1500 rpm for 10 min, and the pelleted VSMCs were collected and incubated with 2 mL DMEM supplemented with 10% FBS and 1% penicillin/streptomycin at 37°C for a week or until 70% confluence. Cells from passage 3 to 6 were used for all experiments.

Synthesis of peptide amphiphiles.

CCR2-binding peptides derived from monocyte chemoattractant protein-1 (MCP-1) and scrambled MCP-1 peptides were conjugated onto DSPE-PEG(2000)-maleimide using a previously reported protocol developed by our lab [19]. Briefly, 0.25 mmol MCP-1 peptide [YNFTNRKISVQRLASYRRITSSK] or scrambled peptide (NT) [YNSLVFRIRNSTQRKYRASIST] were synthesized on an automated peptide synthesizer (PS3, Protein Technologies, Tucson, AZ) on Wang resin *via* standard Fmoc-mediated, solid phase peptide synthesis methods. To cleave the peptide from the resin, a solution of 94:2:5:2:5:1 vol% trifluoroacetic acid:1,2-ethanedithiol:water:triisopropylsilane was added to the beads and reacted for 4 hours. Peptides were dried with nitrogen, precipitated, and washed twice with ice-cold diethyl ether. The crude peptides were dissolved and lyophilized.

MCP-1 and scrambled peptides were dissolved in milliQ water and purified on a reverse-phase high performance liquid chromatography system (HPLC, Prominence, Shimadzu, Columbia, MD) using a Luna C8 column (250 × 10 mm ID, 5 μm, Phenomenex, Torrance, CA) and a gradient mobile phase consisting of (A) 0.1% (v/v) formic acid in water and (B) 0.1% (v/v) formic acid in acetonitrile. The initial mobile phase consisted of 100% solvent A at a flow rate of 10 mL/minute. Solvent A was decreased slowly to 0% over 27 minutes and held at this composition for 3 minutes. The gradient was returned to 100% solvent A over 3 minutes and held at this composition for 1 minute for a total run-time of 34 minutes. The column temperature was kept at 55°C. The m/z was characterized by MALDI-TOF/TOF (Bruker, Billerica, MA, USA). The expected m/z peak is $[M+H]^+ = 2890$ (Fig. S1).

The purified peptides were conjugated to DSPE-PEG(2000)-maleimide in pH 7.4 buffered water for 24 hours. The resulting products were purified using a C4 Jupiter column (250 × 30 mm ID, 5 μm, Phenomenex, Torrance, CA) as described above. The expected m/z peak for the peptide amphiphiles are $[M+H]^+ = 5830$ (Fig. S1). Fluorescently-labeled (Cy5, Cy7) amphiphiles were synthesized similarly using DSPE-PEG(2000)-amine through an NHS ester reaction.

Synthesis of DSPE-PEG(2000)-miR-145 mimics.

miR-145 containing the sense sequence, 5’-GUCCAGUUUUCCCAGGAAUCCCU-3’, and control miR (miR-67), containing the sense sequence, 5’-UCACAACCUCCUAGAAAGAGUAGA-3’, were custom ordered from IDT (Coralville, IA), and modified with a thiol group on the 5’ end of the sense (functional) strand for covalent conjugation to the lipid tail. miR-145-SH (MW = 14490 g/mol, 117.5 nmol, 1.70

mg) was added to DEPC-treated water to make 0.1 mM miR-145 solution. Tris(2-carboxyethyl)phosphine (TCEP) was added to the miR-145 solution and stirred in the dark at room temperature for 4 hours at 1600 rpm. Thiolated miR-145 was conjugated to DSPE-PEG(2000)-malemide (Avanti Polar Lipids, Alabaster, AL) *via* a thioether bond by adding a 10% molar excess of lipid to reduced thiolated miR in DEPC-treated water. The resulting products were characterized using MALDI. The expected m/z peaks for DSPE-PEG(2000)-miR-145 and DSPE-PEG(2000)-miR-67 were $[M+H]^+$ = 17047 and 17717, respectively (Fig. S1).

Construction and characterization of miR-containing micelles.

miR-145 micelles were self-assembled by combining MCP-1 peptide amphiphiles (MCP-1 PA) and DSPE-PEG(2000)-methoxy in a 49:50 mol ratio in methanol. The solvent was completely evaporated under nitrogen and further vacuum dried overnight. The resulting film was hydrated with 100 μL of the solution of DSPE-PEG2000-miR-145 (1 mol%) in nuclease-free water or PBS, and incubated at 60°C for 30 min. After incubation, the micelle solution was cooled to room temperature prior to use. For fluorescence studies, DSPE-PEG(2000)-Cy5 or -Cy7 were incorporated into micelles at a 49:40:10:1 mol ratio of MCP-1 PA, DSPE-PEG(2000)-methoxy, Cy5 or Cy7 amphiphiles, and DSPE-PEG2000-miR-145, respectively. Control micelles containing MCP-1 and miR-67 amphiphiles or scrambled MCP-1 and miR-145 amphiphiles were synthesized in a similar manner for miR-67 micelles and NT miR-145 micelles, respectively.

The particle size and zeta potential of micelles at 100 μM were determined by a Mobius Zetasizer (Wyatt, Santa Barbara, CA), and measurements were carried out in 25°C in three replicates. Transmission electron microscopy (TEM) was used to observe the morphology of miR-145 micelles. Briefly, 100 μM micelle solutions in water were placed on carbon grids (Ted Pella, Redding, CA) and stained with 2 wt% uranyl acetate. Dried samples were imaged on JEM 2100-F (JEOL Ltd., Tokyo, Japan).

miR-145 micelle protection against nucleases.

miR-145 micelles, miR-145 amphiphiles (below critical micelle concentration (CMC)), or free miR-145 containing 10 μg miR were incubated with 20 μL nuclease-treated fetal bovine serum (FBS) for 0.5, 1, 4, and 24 hours at 37°C. The integrity of miR-145 was observed by gel electrophoresis on a 2% (w/v) agarose gel at 56V for 1 hour. Lanes were loaded with miR-145 micelles, miR-145 amphiphiles (below the CMC), or free miR-145 at 10 μg/mL. The gel was imaged on a ChemiDoc XRS+ (Bio-Rad Laboratories, Hercules, CA). The intensity of each band was quantified *via* ImageJ and normalized against untreated miR-145 micelles or free miR-145.

In vitro miR-145 micelle binding assay.

miR-145 micelles or NT miR-145 micelles (100 μM) were incubated with hASMCs for 4 hours to assess binding. Cells were fixed with 4% PFA and blocked with 1% BSA, 22.52 mg/mL glycine, and 0.1% Tween-20 for 1 hour before incubation with anti-CCR2 primary antibodies for 1 hour (Abcam, Cambridge, UK). Cells were incubated for 1 hour in the dark with a secondary antibody labeled with Alexa Fluor 594 (Thermo Fisher Scientific,

Waltham, MA, USA) and counter-stained with DAPI (1 μg/mL) and imaged (Confocal Laser Scanning Microscope 780, Zeiss, Oberkochen, Germany). Competition assays were performed on patient-derived VSMCs. VSMCs were incubated with PBS, MCP-1 peptide, or scrambled MCP-1 peptide for 1 hour at 1 mM concentrations. Cell media and peptide solution were removed and VSMCs were then incubated with miR-145 micelles or NT miR-145 micelles (100 μM). Cells were washed, nuclei stained with DAPI and imaged using a fluorescence microscope (Leica DMi8, Leica, Wetzlar, Germany).

In vitro micelle internalization mechanism.

hASMCs were seeded onto glass coverslips in a 6-well plate for 24 hours at 37°C and 5% CO_2. Cells were incubated with endocytosis and cell uptake inhibitors, including genistein (200 μg/mL, caveolae-mediated endocytosis inhibitor), methyl-β-cyclodextrin (me-β-CD, 50 μM, lipid-raft-mediated endocytosis inhibitor), chlorpromazine (10 μg/mL, clathrin-mediated endocytosis inhibitor), wortmannin (50 nM, macropinocytosis inhibitor), and NaN_3 (10 mM, energy-dependent endocytosis inhibitor), for 30 minutes before fresh media replacement, and cells were washed with PBS and incubated with Cy5miR-145 micelles for 4 hours at 37°C. Cells were transfected with siRNA caveolin I (Thermofisher, Waltham, MA) using Lipofectamine 2000 (Invitrogen, Carlsbad, CA) following manufacturer's protocol. Briefly, Lipofectamine reagent was added to Opti-MEM Medium in which siRNA caveolin I was diluted. This mixture was incubated with cells for 72 hours before Cy5miR-145 micelle uptake was measured. Cells were stained with DAPI (1 μg/mL) and imaged on a Confocal Laser Scanning Microscope 780 (Zeiss, Oberkochen, Germany) at an excitation wavelength of 405 nm and 650 nm to visualize the nucleus (blue) and the micelle internalization (red), respectively.

Cy5miR-145 micelles (100 μM) and cholera toxin subunit B (CT-B) Alexa Fluor488 (5 μg/mL) (caveolae-dependent pathway internalization) were simultaneously incubated with VSMCs for 2 hours at 37°C for assessment of caveolae-mediated endocytosis. The cells were stained with DAPI and observed for intracellular fluorescence distribution using a Confocal Laser Scanning Microscope 780 (Zeiss, Oberkochen, Germany).

In vitro endosomal escape.

To test endosomal escape, hASMCs were incubated at a cell density of 3×10^5 cells/well in Medium 231 (5% SMGS, 1% pen/strep) for 24 hours in 6-well plates containing coverslips. Fluorescently-labeled micelles were incubated for 0.5, 1, 2, and 4 hours. The cell suspensions were washed with PBS, fixed with 4% paraformaldehyde, and stained with Lysotracker Green and DAPI, according to manufacturer's instructions. The cells were observed by a Confocal Laser Scanning Microscope 780 (Zeiss, Oberkochen, Germany) at excitation wavelengths of 405 nm, 504 nm, and 650 nm to visualize the nuclei (blue), acidic compartments of lysosome (green), and micelle internalization (Cy5, red), respectively.

To test the proton sponge effect, hASMCs were seeded in 24-well plates containing coverslips for 24 hours. Bafilomycin A1 (200 nM, V-ATPase inhibitor) was incubated with hASMCs for 45 minutes prior to incubation of miR-145 micelles or PBS for 4 hours in FBS-free Medium 231. After 4 hours, the cells were replenished with Medium 231 supplemented

with SMGS growth medium for an additional 20 hours, prior to PCR analysis of KLF-4, ELK-1, and α-SMA. The co-localization between the endosome/lysosome compartment and Cy5miR-145 micelles were further visualized by confocal microscopy over 0.5, 1, 2, and 4 hours, as described above.

In vitro release profiles.

To evaluate the release of miR-145, miR-145 micelles consisting of 1 μg Alex Fluor647(AF647)-labeled miR-145 were incubated in PBS at 37°C while stirring and supplemented with 4.5 μM glutathione (GSH) or 10 mM GSH to stimulate the extracellular and intracellular reducing environments, respectively. At 0, 0.5, 2, 3.5, 5, 24, and 48 hours, 5 μL of samples were injected in the HPLC (Prominence, Shimadzu, Columbia, MD) to separate free and conjugated form of miR-145 and quantified for free miR content at λ_{ex} = 650 nm.

In vitro mRNA expression.

hASMCs were incubated with nanoparticles or free miRs at a miR concentration of 250 nM in serum-free media. Following the 4 hours transfection period, the media was replaced by supplemented media containing 5% SMGS and incubated for an additional 20 hours. RNA was isolated *via* Trizol (Invitrogen, Carlsbad, CA), and cDNA was synthesized using the RT^2 First Strand Kit (Qiagen, Hilden, Germany) based on manufacturer's instructions. Myocardin, α-SMA, calponin, KLF-4/5, and ELK-1 expressions were determined by real time-PCR using RT^2 SYBR Green qPCR Mastermix (Qiagen, Hilden, Germany) on a CFX384 Real-Time PCR Detection System (Bio-Rad Laboratories, Hercules, CA). GAPDH was used as an internal loading control. The $2^{-\Delta\Delta C_T}$ method was used to quantify mRNA expression level.

miR-145 expression and VSMC phenotypic markers on patient-derived VSMCs.

VSMCs derived from patients were treated with miR-145 micelles and other micelle and miR groups (250 nM miR). Native miR-145 expression, treated VSMC miR-145 expression and VSMC phenotypic markers were analyzed by qRT-PCR.

Functional assays on VSMCs.

Cholesterol efflux and migration assays were performed on patient-derived diseased VSMCs to assess the effect of miR-145 micelles in promoting contractile VSMC function. To assess cholesterol efflux, VSMCs were activated with 10 μg/ml of cholesterol-methyl-β-cyclodextrin for 72 hours. Then, following the manufacturer's protocol (Abcam, Cambridge, United Kingdom), VSMCs were loaded overnight with fluorescently-labeled cholesterol before treatment with miR-145 micelles, free miR-145, free miR-67, or MCP-1 peptide for 5 hours (N=3). The amount of cholesterol effluxed out of cells was quantified using fluorescence readings.

Additionally, a migration assay was performed on VSMCs derived from patients with atherosclerosis. Cells were grown to confluence before treatment with miR-145 micelles, miR-67 micelles, NT miR-145 micelles, free miR-145, free MCP-1 peptide, or PBS for 4 hours. Afterwards, a wound in the monolayer of cells was created with a pipette tip and cells

migrating into the wound region were imaged using a fluorescence microscope (Leica DMi8, Leica, Wetzlar, Germany). Cells were counted after 24 hours using brightfield images and quantified with ImageJ.

In vivo prevention of early-stage atherosclerosis.

Eight-week old, male (N = 15) or female (N = 15) ApoE$^{-/-}$ mice (Jackson Laboratory) were placed on a Western diet (21% (wt/wt) fat, 0.2% (wt/wt) cholesterol, 19.5% (wt/wt) casein, and no sodium cholate. After 2 weeks of Western diet, mice were intravenously injected with miR-145 micelles, miR-67 micelles, NT miR-145 micelles, free miR-145 (1 mg/kg miR (or 0.7 mM total micelle)), or PBS *via* tail vein (N = 6). The mice remained on Western diet for two additional weeks before euthanasia and evaluating serum concentrations of tumor necrosis factor-α (TNF-α) and IL-6 *via* enzyme-linked immunosorbent assay (ELISA, R&D Systems, Minneapolis, MN). The study protocol was reviewed and approved by the Institutional Animal Care and Use Committee (IACUC) at the University of Southern California.

In vivo efficacy studies on mid-stage plaque prevention and growth.

Eight-week old male (N = 54) or female (N = 54) ApoE$^{-/-}$ mice (The Jackson Laboratory, Bar Harbor, ME) were placed on a Western diet for 14 weeks prior to treatment of miR-145 micelles, miR-67 micelles, NT miR-145 micelles, free miR-145 (1 mg/kg miR (or 0.7 mM total micelle)), or PBS *via* tail vein once every three days for 15 days (5 injections). Mice remained on Western diet during treatment period. To check for targeting, micelles were modified to include 10 mol% DSPE-PEG(2000)-Cy7 for the last injection.

In vivo gene expression.

Mice were euthanized and aortas were perfused with PBS. The aortic root region was harvested, weighed, and lysed with Trizol (Invitrogen, Carlsbad, CA). miR was extracted from aortas of ApoE$^{-/-}$ mice by miRNeasy Mini Kit (Qiagen, Hilden, Germany) and linearly amplified with RT^2 miR First Strand Kit (Qiagen, Hilden, Germany), according to manufacturer's instructions. Real-time PCR was conducted on LightCycler 480 Real-Time PCR System (Bio-Rad Laboratories, Hercules, CA) to evaluate cellular miR-145, myocardin, α-SMA, calponin, KLF-4/5, and ELK-1 mRNA levels. GAPDH was used as an internal loading control. The $2^{-\Delta\Delta C}{}_T$ method was used to calculate relative expression changes.

Ex vivo aorta imaging and *en face* oil red O (ORO) staining.

Aortas were excised and fluorescently imaged to detect particle fluorescence signal. Next, aortas were fixed in 4% paraformaldehyde overnight at 4°C. Excess adventitial fat on aortas was removed under a stereomicroscope and the tissue was washed in PBS. Aortas were then washed in 78% methanol for 5 minutes 3 times before incubating in 2% ORO solution for 60 minutes. Aortas were then washed again in 78% methanol twice and cut open longitudinally before imaging. Plaques were measured and quantified by detecting positively stained areas (red) with ImageJ software.

Histology and immunohistochemistry.

Aortic roots and aortas excised from mice and perfused with PBS were embedded and frozen in OCT at −80°C. Aortic roots were sectioned (5 μm) where the aortic valve leaflets were present. To assess plaque size, necrotic core, and collagen content, serial cross-sections of the aortic root were stained with hematoxylin and eosin (H&E), oil red o (ORO), or picrosirius red, respectively (Abcam, Cambridge, United Kingdom) and every 10th section was measured using ImageJ software. To detect Cy7-labeled micelles, aortic sections were stained with DAPI and imaged using the Confocal Laser Scanning Microscope 780 (excitation: 730 nm; emission: 783 nm, Zeiss, Oberkochen, Germany).

For immunohistochemistry staining, aortic root sections were washed with Tris Buffered Saline (TBS) containing 0.025% Triton X-100. The sections were blocked with 1% BSA, 10% normal goat serum, 0.3 M glycine in 0.1% TBS Tween-20 for 1 h at room temperature, followed by incubation with anti-alpha smooth muscle actin (Abcam) and anti-CD68 (Abcam) overnight at 4°C in a humidified chamber. The sections were washed and rinsed with TBS, prior to 1 hour incubation with Alexa Fluor 594 goat anti-rabbit IgG (Thermo Fisher Scientific, Waltham, MA) at room temperature in the dark. The samples were counterstained with DAPI and mounted with a coverslip using VectaMount™ aqueous mounting medium (Vector Laboratories, Burlingame, CA). Stained sections were imaged using a fluorescence microscope (Leica DMi8, Leica, Wetzlar, Germany).

In vivo evaluation of micelle biocompatibility and toxicity.

Toxicity of miR-145 micelle, miR-67 micelle, NT miR-145 micelle, free miR-145, or PBS was evaluated at the conclusion of the pharmacokinetics studies. Briefly, heart, lung, liver, kidney, and spleen were harvested and fixed with formalin overnight at 4°C, before submerging in 30% sucrose solution for 8 hours and embedding in OCT at −80°C. OCT-embedded 5 μm tissue sections were stained with H&E and imaged to discern any morphological signs of tissue damage. In addition, weight changes of mid-stage atherosclerotic mice were monitored during treatment. Blood urea nitrogen (BUN, Bioo Scientific, Austin, TX, USA) and urine creatinine (Crystal Chem, Elk Grove Village, IL, USA) levels were measured in mouse serum and urine following manufacturer's protocols to assess any renal toxicity (N = 6).

In vivo pharmacokinetics and biodistribution.

Wild type, eight-week old male (N = 4) C57B1/6J mice (Jackson Laboratory, Bar Harbor, ME) were intravenously injected with miR-145 micelles containing 10 mol% Cy7 amphiphiles and AF647 miR-145 at a miR dose of 1 mg/kg. Blood was collected at 5 minutes, 1, 3, 8, and 24 hours by orbital sinus, tail vein, or cardiac puncture. Whole blood was centrifuged at 12,000 rpm for 4 minutes to obtain the serum, and miR-145 and amphiphile concentrations were determined by fluorescence measurements (miR-145: excitation: 650 nm; emission: 670 nm and Cy7 amphiphiles: excitation: 730 nm; emission: 783 nm).

At 24 hours, the mice were euthanized and the brain, heart, lung, liver, kidneys and spleen, were resected and the biodistribution of micelles were quantified by optical imaging

(amiHTX, Spectral Instruments Imaging, Tucson, AZ). Signal from the PBS group was used as background measurements.

Statistical analysis.

Results were expressed as means ± standard deviation (S.D.). A two-tailed Student *t*-tests was used to determine statistical significance between two groups, while a one-way analysis of variance (ANOVA) was used to determine statistical significance between more than two groups. A p value < 0.05 was considered statistically significant. All statistical analyses were conducted using GraphPad Prism 8 (GraphPad Software, San Diego, CA).

Results

Synthesis and characterization of miR-145 micelles

To synthesize miR-145 micelles, miR-145 mimics were thiolated on the 5' end of the sense (functional) strand and covalently conjugated to DSPE-PEG(2000)-maleimide *via* a thioether linkage (Fig. S1). The resulting miR-145 amphiphiles were mixed with MCP-1 peptide amphiphiles that target CCR2 and DSPE-PEG(2000)-methoxy to self-assemble miR-145 micelles (Fig. 1A) [7, 20–24]. For fluorescence studies, Cy7 amphiphiles were included at 10 mol%. TEM images showed miR-145 micelles are monodisperse and spherical nanoparticles (Fig. 1B), and the hydrodynamic diameter and surface charge were measured to be 21.7 ± 2.2 nm and 15.1 ± 0.2 mV by dynamic light scattering (DLS) and zeta potential measurements, respectively (Fig. 1C). miR-67, which is not expressed in mice or humans, and scrambled MCP-1 peptides were used to synthesize non-therapeutic miR-67 micelles and non-targeting (NT) miR-145 micelles, respectively, and served as controls (Fig. S2, Table 1). As shown in Table 1, the addition of miR amphiphiles into micelles increased the size of the nanoparticles compared to MCP-1 micelles only (14.6 ± 4.2 nm). Nonetheless, surface charge and polydispersity index of the particles remained similar (Table 1).

To verify miR-145 was incorporated into micelles, gel shift assays were conducted, and the mobility of miR-145 micelles was assessed (Fig. 1D). Upon electrophoresis, miR-145 micelles remained within the well and did not show migration down the gel (Lane A), indicating miR-145 was incorporated into the micelle at concentrations above the critical micelle concentration (CMC, 2 μM) [25]. In contrast, when miR-145 amphiphiles were loaded at 0.6 μM, or below the CMC, as expected, micelles did not assemble and the band containing miR-145 amphiphiles readily migrated down the gel similar to free miR-145 (Lane B and C, respectively). In addition, when gel shift assays were performed with miR-145 micelles in the presence of nucleases, miR-145 degradation was significantly inhibited over 24 hours, retaining 89.6 ± 4% of the miR signal in the well (Lane 3). However, without the protection of the micelle, free miR-145 amphiphiles (below the CMC) and free miR-145 migrated down the gel and only 38.2 ± 1% and 29.2 ± 20.8% remained by 24 hours, respectively (Lane 4 and 5). In contrast, untreated miR-145 micelle, untreated miR-145, and FBS only, respectively (lanes 1, 2, and 6, Fig. 1D), showed no degradation of miRs without nuclease treatment.

Binding, internalization, and endosomal escape of miR-145 micelles

To verify the binding of miR-145 micelles to VSMCs, we incubated VSMCs with miR-145 micelles for 4 hours. Upon staining for CCR2, we found that miR-145 micelles colocalized with CCR2 expression (Fig. 2A). However, binding was not observed for NT miR-145 micelles (Fig. 2B). To further corroborate that the binding of miR-145 micelles is due to CCR2-binding peptides derived from MCP-1, we preincubated patient VSMCs with scrambled MCP-1 peptide or MCP-1 peptide, before treatment with miR-145 micelles or NT miR-145 micelles (Fig. 2C) [26,27]. Unlike scrambled MCP-1 peptides, miR-145 micelle binding was reduced upon MCP-1 peptide preincubation, given that the binding sites were likely saturated with the peptide.

To determine the mechanism of intracellular uptake, we incubated hASMCs with endocytosis pathway inhibitors before miR-145 micelle treatment and assessed nanoparticle uptake. As shown in Figure 3, hASMCs incubated with genistein (caveolae-mediated endocytosis inhibitor) and methyl-β-cyclodextrin (me-β-CD, lipid raft-mediated endocytosis inhibitor) showed a significant decrease in micelle internalization. In addition, hASMCs were also incubated with internalization inhibitors: chlorpromazine (clathrin-mediated endocytosis inhibitor), wortmannin (macropinocytosis inhibitor), and sodium azide (energy-dependent endocytosis inhibitor, NaN_3, Fig. S3). Only hASMCs incubated with genistein, me-β-CD, and sodium azide showed a significant decrease in micelle internalization suggesting that miR-145 micelles enter cells *via* energy-dependent, caveolae-mediated lipid rafts. This was further confirmed when miR-145 micelle uptake decreased after hASMCs were transfected with caveolin I siRNA (Fig. 3A) and, through colocalization studies using cholera toxin subunit-B (CT-B) Alexa Fluor488, a protein known for internalization *via* caveolae-mediated endocytosis (Fig. 3B) [28].

In order to ensure miR cargo delivery to the cytosol, nanoparticles need to escape the endosome after cell uptake [29]. To demonstrate endosomal escape of miR-145 micelles, hASMCs were incubated with Cy5-labeled, miR-145 micelles (Cy5miR-145 micelle) for up to 4 hours and endosomes were stained with Lysotracker Green. Although colocalization of miR-145 micelles with endosomes was found at 30 minutes (punctate yellow signal, Fig. 3C), 88% of Cy5miR-145 micelles (red) were found to be present in the cytosol by 4 hours (Fig. 3C, 3D). Similar to other cationic nanoparticles, the successful endosomal escape of miR-145 micelles may be attributed to the proton sponge effect in which the charge of the micelles induces swelling of endosome and release of its contents [30]. This hypothesis was verified through the treatment of hASMCs with miR-145 micelles in the presence of the vacuolar proton pump inhibitor, bafilomycin A1, which prevents the acidification of lysosomes. As shown in Figure 3C and D, incubation with bafilomycin A1 led to 82–94% retention of miR-145 micelles within the endo-lysosomal compartment throughout the 4-hour incubation period. As such, no changes in synthetic and contractile marker expression were found (Fig. S4).

Once inside the cytoplasm, intracellular concentrations of glutathione (GSH, 10 mM) can act as a natural reducing agent that can cleave thioether bonds like those found between miR-145 and PEG to release therapeutic cargo [31–33]. To assess whether miR-145 is released from micelles using this mechanism, we incubated miR-145 micelles containing

AF647-labeled miRs with 10 mM cytosolic GSH concentrations or 4.5 μM GSH, correlating with extracellular GSH concentration, for up to 48 hours [31–33]. While 19% of miR-145 was released from miR-145 micelles in environments with 4.5 μM GSH, 100% of miR-145 was released by 4 hours under cytosolic GSH concentrations, suggesting premature release of miR-145 is minimal prior to cell internalization (Fig. 3E) [34, 35]. Overall, these results indicate that miR-145 micelles are uptaken by VSMCs and successfully release the miR cargo in the cytosol for post-transcriptional gene regulation.

Modulation of atherosclerotic genes *in vitro* and in VSMCs derived from patients with cardiovascular disease

After validation of successful miR-145 micelle uptake and release, we investigated the efficacy of miR-145 micelles to modulate VSMC phenotype. As miR-145 promotes athero-protection by regulating the contractile phenotype and inhibiting the synthetic VSMC phenotype, we incubated hASMCs with miR-145 micelles for 4 hours and evaluated SMC markers through qRT-PCR [8]. As shown in Figure S5, miR-145 micelles upregulated the contractile genes, myocardin (162.1 ± 10.7%), α-SMA (166.7 ± 12.5%), and calponin (142.5 ± 18.2%, Fig. S5A) and simultaneously downregulated synthetic genes, KLF-4/5 and ELK-1 expression (KLF-4: 44.3 ± 5.3%, KLF-5: 56.5 ± 6.2%, ELK-1: 30.4 ± 1.8%, relative to PBS treatment groups, Fig. S5B). Free miR-145 also had a minor effect and upregulated contractile genes myocardin (132.9 ± 5.9%), α-SMA (149.4 ± 12.9%), and calponin (121.1 ± 13.0%), and downregulated synthetic genes KLF-5 (72.1 ± 15.1%), KLF-4 (54.5 ± 5.5%), and ELK-1 (37.5 ± 15.5%), which is consistent with other *in vitro* studies [36].

In addition, we tested the expression of endogenous miR-145 and the efficacy of miR-145 micelles on VSMCs isolated directly from atherosclerotic or healthy arteries discarded from patients undergoing vascular surgery (Fig. 4A) [7, 37]. Consistent with previous reports, miR-145 was 56.4 ± 16.8% lower in VSMCs derived from diseased arteries compared to VSMCs from healthy arteries (Fig. 4B) [7, 37]. As such, contractile markers myocardin (14.2 ± 3.2%) and calponin (27.2 ± 5.0%) were downregulated, while synthetic markers KLF-5 (196.9 ± 31.8%) and ELK-1 (158.8 ± 26.6%) were overexpressed in VSMCs derived from diseased tissue compared to healthy tissue (Fig. 4C). Consistent with Figures S5A and S5B, when patient-derived VSMCs from diseased tissue were treated with miR-145 micelles, the expression of contractile markers myocardin (151.8 ± 26.0%), α-SMA (180.3 ± 26.5%), and calponin (158.8 ± 21.6%) increased, while synthetic markers KLF-5 (65.3 ± 8.2%) and ELK-1 (74.9 ± 9.8%) significantly decreased relative to PBS controls (Fig. 4D). NT miR-145 micelles and free miR-145 also showed an increase in myocardin expression, but no statistical differences in calponin, and KLF-5 and ELK-1 were found compared to PBS controls.

After verifying miR-145 micelles increased contractile gene expression, functional assays were performed to investigate the effects of miR-145 micelles to promote the contractile function in diseased patient-derived VSMCs. To assess this, VSMCs were treated with methyl-β-cyclodextrin cholesterol to activate the cells into an atherogenic state for 72 hours. After activation, the cells were treated with miR-145 micelles, free miR-145, free miR-67, or MCP-1 peptide, and the amount of cholesterol effluxed out of the cells was measured over 5

hours (Fig. S6A). miR-145 micelle treatment induced the most cholesterol efflux (80.5 ± 1.6%), followed by free miR-145 (63.6 ± 9.4%, *p < 0.05), miR-67 (55.2 ± 1.8%, **p < 0.01), and the MCP-1 peptide negative control (58.1 ± 11.2%, **p < 0.01), confirming miR-145 delivery by micelles promotes the contractile phenotype and thereby suggests, miR-145 micelles can decrease foam cell transition. [38]. Furthermore, using a wound healing assay, we also demonstrate that miR-145 micelles inhibited migration of VSMCs when compared to miR-67 micelle treatment, NT miR-145 micelle treatment, free miR-145 and non-treated controls (miR-145 micelles: −42.1 ± 24% vs 3.8 ± 46.1%, −16.2 ± 37.4% −9.3 ± 35.4%, respectively, *p < 0.05 when compared to PBS, Fig S6B). In this case, MCP-1 peptide served as a positive control and increased cell migration (40.8 ± 46.5%, *p < 0.05). Thus, collectively, these results demonstrate that micelle nanoparticles enhance miR-145 uptake by VSMCs and can rescue the contractile phenotype.

Early atherosclerosis prevention by miR-145 micelles *in vivo*

We next sought to determine the viability of miR-145 micelles as a therapeutic for atherosclerosis *in vivo*. As mentioned, synthetic VSMCs overproliferate and migrate, and can transdifferentiate to alternative cell types such as macrophages, foam cells, and osteochondrogenic cells that make up the majority of atherosclerotic plaques. Hence, we tested whether modulating VSMCs through miR-145 micelle treatment at an early disease stage could act as a therapeutic strategy to inhibit plaque formation and disease progression [39]. To test this, ApoE$^{-/-}$ mice were fed a high-fat diet for two weeks to represent a pre-disease state. Afterwards, mice were treated with one dose of miR-145 micelles, miR-67 micelles, NT miR-145 micelles, free miR-145 (1 mg/kg miR dose), or PBS and subjected to two additional weeks of high fat diet. At the end of four weeks, aortas were collected from mice for histological analyses and VSMCs were isolated from aortic tissue for qRT-PCR (Fig. S7). As shown in Figure 5A, miR-145 micelles increased expression of miR-145 to 178.5 ± 22.9% (vs. PBS, **** p < 0.0001), whereas no change in miR-145 expression was observed for mice treated with other groups. Notably, the increased expression of miR-145 provided by miR-145 micelles induced contractile SMC gene expression (179.4 ± 25.5%, **** p < 0.0001; 141.9 ± 7.9%, *** p < 0.001; and 180.1 ± 11.4%, **** p < 0.0001; for myocardin, α-SMA, and calponin, respectively, vs. PBS, Fig. 5B). Likewise, miR-145 micelle treatment reduced synthetic SMC marker expression including KLF-5, KLF-4, and ELK-1 to 58.0 ± 7.0% (*** p < 0.001), 60.2 ± 8.2% (*** p < 0.001), and 53.2 ± 3.6% (**** p < 0.0001), respectively. In contrast, mice treated with miR-67 micelles, NT miR-145 micelles, and free miR-145 exhibited no statistical differences in expression of contractile or synthetic markers relative to PBS-treated controls. These results strongly suggest that early dosing of VSMCs with miR-145 micelles can prevent VSMCs from adopting the synthetic phenotype that contributes to atherogenesis.

As larger necrotic cores and thinner fibrous caps are associated with unstable plaques, we further analyzed and quantified the structure of plaques through histological cross sections of the ascending aorta [40, 41]. Notably, in mice treated with miR-145 micelles, two out of the six aortas did not contain any plaques, which was not seen in any other groups. To compare the effects of treatments on plaque structure and morphology, histological analyses were limited to aorta from mice that contained plaques. Compared to the PBS-treated mice,

miR-145 micelle-treated mice showed a reduction in lesion size and necrotic core area in the ascending aorta by 49 ± 0.1% (** $p < 0.01$ compared to PBS) and 73 ± 0.3% (*** $p < 0.001$), measured with H&E and oil red O (ORO) lipid stain, respectively (Figs. 5C, 5D, 5E). Picrosirius red collagen staining showed miR-145 micelle treatment significantly enhanced collagen content within atherosclerotic plaques compared to other groups, which is correlated with stable plaques and a thicker fibrous cap (86.3 ± 13.0% of total plaque area, **** $p < 0.0001$). In addition, miR-145 micelles reduced inflammation associated with atherosclerosis and synthetic VSMCs as found through a reduction in serum TNF-α ($p < 0.01$ vs. PBS, Fig. 6A) and IL-6 cytokines ($p < 0.05$ vs. PBS, Fig. 6B) to levels similar to that of C57BL/6J mice on a standard diet [42]. Thus, miR-145 micelles demonstrated therapeutic efficacy in preventing early plaque propagation through VSMC phenotypic modulation and associated plaque development.

Atherosclerosis inhibition by miR-145 micelles in advanced stages—In addition to inhibiting disease progression in early-stage atherosclerotic mice, to test the potential of miR-145 micelles to be applied and intervene during later stages of the disease, mid-stage atherosclerotic ApoE$^{-/-}$ mice were established through a high fat diet for 14 weeks [43]. At week 14, mice were administered 5 doses of miR-145 micelles once every three days over three weeks, while remaining on a high fat diet (17 weeks total of high fat diet, Fig. S8). Twenty-four hours after the last injection, whole aortas were excised, prepared en face, and stained with ORO to assess the size and coverage of plaques throughout the aorta. As shown in Figure 7A and B, mice treated with miR-145 micelles showed the least amount of plaques (20.0 ± 4.5% of plaques to total aorta surface area) compared to all control groups (miR-67 micelle: 29 ± 5.9%; $p = 0.0014$ vs. NT miR-145 micelle: 35.6 ± 10.3%; free miR-145: 25.4 ± 4.7%; $p = 0.0004$ vs. PBS: 40.0 ± 6.4%). Histological analyses of the plaques were performed on aortic root sections stained with H&E, ORO, and picrosirius red. As shown in Figure 7C–E, miR-145 micelle-treated mice correlated with a decrease in atherosclerotic plaque lesion size and necrotic core area by 43% and 72%, respectively (vs. PBS-treated controls, $p < 0.001$ and $p < 0.0001$). Picrosirius red collagen stains showed miR-145 micelle treatment preserved the most intraplaque collagen (44.6 ± 3.1% collagen area of total plaque area vs. PBS: 13.5 ± 2.9%, $p < 0.0001$, Fig. 7F), while mice in PBS, miR-67 micelle, NT miR-145, and free miR-145 treatment groups developed larger plaques, exhibited increased necrotic core area, and had lower collagen content in the fibrous cap, characteristic to rupture-prone plaques [40]. No statistical significance was found among miR-67 micelles, NT miR-145 micelles, free miR-145, and PBS treatment groups.

In addition, using immunohistochemistry, expression of α-SMA as well as CD68, an inflammatory monocyte/macrophage marker, was analyzed in plaques to determine the level of contractile VSMCs vs. inflammatory monocytes/macrophages in aortic roots, respectively (Fig. S9). miR-145 micelle treatment of mid-stage atherosclerotic mice showed an increase in α-SMA expression, whereas PBS, free miR-145, NT miR-145 micelle, and miR-67 micelle treatment showed little α-SMA expression. Notably, α-SMA expression in plaques of miR-145 micelle treated mice was found throughout the plaque area whereas α-SMA expression in other groups remained confined to the media regions of the artery (Fig S8). In contrast, miR-145 micelle treatment showed the least expression of CD68 and CD68

expression was concentrated in the fibrous cap region of the plaques in PBS, free miR-145, and NT miR-145 micelle treated mice. Together, these histological analyses demonstrate that miR-145 micelles are efficacious in promoting the contractile VSMC phenotype *in vivo* at later stages of the disease.

In addition, miR-145 micelle treatment showed a significant increase in miR-145 expression (140.3 ± 21.6% vs. 192.7 ± 60.8% for miR-145 micelles vs. baseline groups sacrificed at week 14) in the aortic root and upregulation of contractile markers (myocardin: 145.4 ± 20.4% vs. 151.6 ± 17.2%; α-SMA: 200.4 ± 43.9% vs. 221.4 ± 24.4%; calponin: 167.8 ± 24.7% vs. 177.2 ± 18.3% for miR-145 micelles vs. baseline all relative to PBS), as well as downregulation of synthetic markers (KLF-5: 63.1 ± 11.8% vs. 68.3 ± 11.1%; KLF-4: 83.6 ± 8.1% vs. 92 ± 10.8%; ELK-1: 69.6 ± 9.2% vs. 71.6 ± 31.2% for miR-145 micelles vs. baseline all relative to PBS; Figs. 7G and 7H). No statistically significant differences in miR-145 expression and contractile or synthetic markers were observed for other treatment groups. Thus, we highlight the efficacy of miR-145 micelles to promote healthy, contractile VSMC phenotypes and thereby significantly restricting plaque growth and atherosclerosis progression in mid-stage disease models.

miR-145 micelles targeting to plaques and biocompatibility in vivo

To confirm targeting by miR-145 micelles to atherosclerotic plaques, 24 hours after the final injection in the mid-stage in vivo study, whole aortas were excised and fluorescently imaged. Ex vivo fluorescence images of whole aortas showed the most particle signal for miR-145 micelles ($3.5 \times 10^7 \pm 9.9 \times 10^6$ AU), followed by miR-67 micelles ($1.4 \times 10^7 \pm 6.0 \times 10^6$ AU) and NT miR-145 micelles ($2.9 \times 10^7 \pm 6.1 \times 10^6$ AU), indicating that MCP-1 peptides facilitated enhanced plaque targeting (Fig. 8A). Some nonspecific diffusion of NT miR-145 micelles into the plaques can be attributed to endothelium disruption that is commonly observed in atherosclerotic plaques [44]. However, no fluorescence signal was detected in the aorta of mice treated with free miR-145 and was similar to PBS controls (Figs. 8A). This result is further confirmed by histological analyses of artery cross-sections that showed the Cy7 particle signal confined to atherosclerotic plaques (Fig. 8B).

When biodistribution and pharmacokinetic properties were assessed, miR-145 micelles were found to be primarily eliminated by the liver, in accordance with other micellar systems, and remain co-assembled during circulation at 24 hours (Fig. S10A–S10F). Nonetheless, no signs of tissue necrosis and morphological changes (Fig. 9A) were found for all major organs when compared to non-treated groups, and there was no loss in body weight, indicating the nanoparticle dosages were well-tolerated during the three weeks of treatment (Fig. 9B). Furthermore, blood urea nitrogen and creatinine levels were similar among all groups and within the range of healthy wild type mice, confirming kidney health and safety of these particles in vivo (Fig. 9C) [25, 45].

Discussion

Herein, we demonstrate the potential of nanoparticle-mediated delivery of miR-145 to VSMCs for atherosclerosis therapy. Specifically, we show that CCR2-targeting peptides facilitate micelle uptake and endosomal escape in VSMCs and upregulate contractile

phenotypes in diseased patient VSMCs. In early stage mouse models of atherosclerosis, we found that miR-145 micelles mitigate plaque growth by promoting the contractile VSMC phenotype through miR-145 delivery. Similarly, miR-145 micelles accumulated in plaques and reduced plaque size and necrotic core area in advanced stage models of atherosclerosis. In addition, miR-145 micelle treatment led to a reduction in inflammatory cytokines and inhibited rupture prone plaques by promoting plaque-stabilizing collagen (Fig. 5–7). Ultimately, we demonstrate that miR-145 micelles promote the contractile VSMC phenotype *in vitro* and *in vivo*, and reduce unstable plaques in atherosclerosis.

The therapeutic effect of miR-145 micelles is most likely multifaceted with additional potential mechanisms of plaque reduction that need further investigation. For instance, it is possible that miR-145 micelles are also delivered to CCR2 expressed on VSMC-derived macrophages, activated endothelial cells, and recruited monocytes involved in atherogenesis [16]. Because recruited monocytes play a large role in propagating and forming the necrotic core of plaques as foam cells, if bound to circulating monocytes, miR-145 micelles can lessen monocyte recruitment and the inflammatory response by potentially saturating chemotactic CCR2 binding sites on the monocytes [47]. This hypothesis is partially supported by the CD68 stains, a marker commonly used to identify monocytes and circulating macrophages, in Fig. S9 that show a reduction of CD68 signal in plaques from advanced atherosclerotic mice treated with miR-145 micelles. However, additional studies will be needed to delineate between VSMC-derived inflammatory cells vs. monocytes that were recruited from circulation into plaques. In addition, miRs are capable of regulating the expression of multiple genes. While we mainly focused on the regulation of KLF-4/5, ELK-1, myocardin, α-SMA, and calponin, miR-145 has been suggested to regulate additional pathways such as calcium fluxes and angiotensin-converting enzyme which may further affect plaque growth [48]. Thus, future studies will investigate the impact of miR-145 micelles on additional CCR2-expressing cells and elucidate additional therapeutic effects of our nanoparticles.

Although we demonstrate the potential of miR-145 micelles for atherosclerosis therapy, we note a few limitations in the current study. In the early atherosclerotic model, the dramatic effect of a single dose of miR-145 micelles in altering miR-145 expression and reducing lesion size is not fully understood (Fig. 5). Recent studies with *in vivo* VSMC lineage tracing showed that the clonal expansion of a few VSMCs in the arterial wall are responsible for most VSMC-derived cells in plaques [49]. Thus, it is possible that early intervention of VSMC proliferation and transdifferentiation into other non-contractile VSMCs is able to significantly impede atherosclerosis plaque development long-term [8]. As such, future studies will investigate the retention of miR-145 micelles in plaques and its sustained effects on VSMCs in longitudinal studies. Finally, although we observed in our *in vitro* experiments using diseased, patient-derived synthetic VSMCs that miR-145 micelles can completely restore the contractile phenotype (Fig. 4), our *in vivo* studies in mid-stage mice showed miR-145 micelles can maintain the baseline levels of atherogenesis but not further regress the disease (Fig. 7). To investigate the full benefits of miR-145 therapy in advanced stages of atherosclerosis, future studies will alter miR-145 dose and increase the duration of treatment. Nonetheless, we highlight the potential of miR-145 micelles as a novel

therapeutic strategy to impede atherosclerosis progression at multiple stages through the regulation of VSMC phenotype.

Conclusion

In summary, we report a novel therapeutic strategy for atherosclerosis using miR-145 micelles. miR-145 micelles target CCR2 expressed on VSMCs and was found to escape the endosome to exert a therapeutic effect *in vitro*. By incorporating miR-145 into micelles, miR-145 protected miRs from premature release extracellularly and degradation by nucleases, a common barrier to nucleic acid delivery. *In vivo*, miR-145 micelles demonstrated reduction in plaque lesion size and necrotic core area, while preserving collagen structure in both early- and mid-stage murine atherosclerosis models. Given the targeting and therapeutic efficacy of miR-145 micelles and its biocompatibility *in vivo*, we report the potential of miR-145 to mitigate atherosclerosis and its promise as a long-term therapy for chronic diseases such as atherosclerosis.

Supplementary Material

Refer to Web version on PubMed Central for supplementary material.

Acknowledgments

The authors thank the Center for Electron Microscopy and Microanalysis, Center of Excellence in NanoBiophysics, Core Center of Excellence in Nano Imaging, and Translational Imaging Center at the University of Southern California for assistance in instrumental setups. We also thank our patients for consenting to donate their tissues for this study.

Funding Sources

This work was support by the University of Southern California, the American Heart Association Predoctoral Fellowship (19PRE34380998) awarded to D.D.C., the National Heart, Lung, and Blood Institute (NHLBI, R00HL124279), New Innovator Award (NIH, DP2-DK121328), Eli and Edythe Broad Innovation Award, the L.K. Whittier Foundation Non-Cancer Translational Research Award, and WISE Gabilan Assistant Professorship granted to E.J.C.

Abbreviations

VSMCs	vascular smooth muscle cells
miR-145	micelles miR-145 containing peptide amphiphile micelles
CCR2	C-C chemokine receptor 2
MCP-1	monocyte chemoattractant protein-1
CCL2	C-C motif chemokine ligand 2
α-SMA	alpha smooth muscle actin
miR	microRNA; KLF-4/5 Krüppel-like factor 4 and 5
ELK-1	ETS domain-containing protein-1
PEG	polyethylene glycol

TEM	transmission electron microscopy
DLS	dynamic light scattering
CMC	critical micelle concentration
FBS	fetal bovine serum
hASMCs	human aortic smooth muscle cells
Me-β-CD	methyl-β-cyclodextrin
Cy5miR-145	micelles Cy5 labeled-miR-145 micelles
CT-B	cholera toxin subunit B
GSH	glutathione
AF647	Alexa Fluor 647
BUN	blood urea nitrogen
SMGS	smooth muscle growth supplement
IACUC	Institutional Animal Care and Use Committee
HPLC	high performance liquid chromatography
HBSS	Hank's balanced salt solution
S.D.	standard deviation

References

1. Brozovich FV, et al., Mechanisms of Vascular Smooth Muscle Contraction and the Basis for Pharmacologic Treatment of Smooth Muscle Disorders. Pharmacol Rev, 2016. 68(2): p. 476–532. [PubMed: 27037223]
2. Bennett MR, Sinha S, and Owens GK, Vascular Smooth Muscle Cells in Atherosclerosis. Circ Res, 2016. 118(4): p. 692–702. [PubMed: 26892967]
3. Gomez D and Owens GK, Smooth muscle cell phenotypic switching in atherosclerosis. Cardiovascular research, 2012. 95(2): p. 156–164. [PubMed: 22406749]
4. Shankman LS, et al., KLF4-dependent phenotypic modulation of smooth muscle cells has a key role in atherosclerotic plaque pathogenesis. Nature Medicine, 2015. 21: p. 628.
5. Basatemur GL, et al., Vascular smooth muscle cells in atherosclerosis. Nature Reviews Cardiology, 2019. 16(12): p. 727–744. [PubMed: 31243391]
6. Wahid F, et al., MicroRNAs: synthesis, mechanism, function, and recent clinical trials. Biochim Biophys Acta, 2010. 1803(11): p. 1231–43. [PubMed: 20619301]
7. Lovren F, et al., MicroRNA-145 Targeted Therapy Reduces Atherosclerosis. Circulation, 2012. 126(11, Suppl. 1): p. S81–S90. [PubMed: 22965997]
8. Cordes KR, et al., miR-145 and miR-143 regulate smooth muscle cell fate and plasticity. Nature, 2009. 460(7256): p. 705–10. [PubMed: 19578358]
9. Elia L, et al., The knockout of miR-143 and −145 alters smooth muscle cell maintenance and vascular homeostasis in mice: correlates with human disease. Cell Death And Differentiation, 2009. 16: p. 1590. [PubMed: 19816508]

10. Fichtlscherer S, et al., Circulating microRNAs in patients with coronary artery disease. Circ Res, 2010. 107(5): p. 677–84. [PubMed: 20595655]
11. Zhou LY, et al., Current RNA-based Therapeutics in Clinical Trials. Curr Gene Ther, 2019. 19(3): p. 172–196. [PubMed: 31566126]
12. Chen Y, Gao D-Y, and Huang L, In vivo delivery of miRNAs for cancer therapy: Challenges and strategies. Adv. Drug Delivery Rev, 2015. 81: p. 128–141.
13. Hoy SM, Patisiran: First Global Approval. Drugs, 2018. 78(15): p. 1625–1631. [PubMed: 30251172]
14. Chin DD, Chowdhuri S, and Chung EJ, Calcium-Binding Nanoparticles for Vascular Disease. Regenerative Engineering and Translational Medicine, 2019. 5(1): p. 74–85. [PubMed: 31106257]
15. Chin DD, et al., Collagenase-Cleavable Peptide Amphiphile Micelles as a Novel Theranostic Strategy in Atherosclerosis. Advanced Therapeutics, 2020. 3(3): p. 1900196.
16. Poon C, et al., Protein Mimetic and Anticancer Properties of Monocyte-Targeting Peptide Amphiphile Micelles. ACS Biomaterials Science & Engineering, 2017.
17. Schecter AD, et al., MCP-1-dependent signaling in CCR2(−/−) aortic smooth *muscle cells*. J Leukoc Biol, 2004. 75(6): p. 1079–85. [PubMed: 15020650]
18. Wang JM, Chen AF, and Zhang K, Isolation and Primary Culture of Mouse Aortic Endothelial Cells. J Vis Exp, 2016(118).
19. Chung EJ, et al., Monocyte-targeting supramolecular micellar assemblies: a molecular diagnostic tool for atherosclerosis. Adv Healthc Mater, 2015. 4(3): p. 367–76. [PubMed: 25156590]
20. Cui H, Webber MJ, and Stupp SI, Self-assembly of peptide amphiphiles: from molecules to nanostructures to biomaterials. Biopolymers, 2010. 94(1): p. 1–18. [PubMed: 20091874]
21. Trent A, et al., Structural properties of soluble peptide amphiphile micelles. Soft Matter, 2011. 7(20): p. 9572–9582.
22. Akinc A, et al., Development of lipidoid-siRNA formulations for systemic delivery to the liver. Mol Ther, 2009. 17(5): p. 872–9. [PubMed: 19259063]
23. Lee T, et al., Dosage and temporal thresholds in microRNA proteomics. Mol Cell Proteomics, 2015. 14(2): p. 289–302. [PubMed: 25467838]
24. Shu J, et al., Dose-dependent differential mRNA target selection and regulation by let-7a-7f and miR-17–92 cluster microRNAs. RNA Biol, 2012. 9(10): p. 1275–87. [PubMed: 22995834]
25. Chung EJ, et al., In vivo biodistribution and clearance of peptide amphiphile micelles. Nanomedicine, 2015. 11(2): p. 479–87. [PubMed: 25194999]
26. Andjelkovic AV and Pachter JS, Characterization of binding sites for chemokines MCP-1 and MIP-1alpha on human brain microvessels. J Neurochem, 2000. 75(5): p. 1898–906. [PubMed: 11032879]
27. Dzenko KA, et al., The chemokine receptor CCR2 mediates the binding and internalization of monocyte chemoattractant protein-1 along brain microvessels. J Neurosci, 2001. 21(23): p. 9214–23. [PubMed: 11717355]
28. Thyberg J, Differences in caveolae dynamics in vascular smooth muscle cells of different phenotypes. Lab Invest, 2000. 80(6): p. 915–29. [PubMed: 10879742]
29. Dowdy SF, Overcoming cellular barriers for RNA therapeutics. Nat Biotechnol, 2017. 35(3): p. 222–229. [PubMed: 28244992]
30. Benjaminsen RV, et al., The possible “proton sponge “ effect of polyethylenimine (PEI) does not include change in lysosomal pH. Mol Ther, 2013. 21(1): p. 149–57. [PubMed: 23032976]
31. Gujrati M, et al., Multifunctional cationic lipid-based nanoparticles facilitate endosomal escape and reduction-triggered cytosolic siRNA release. Mol Pharm, 2014. 11(8): p. 2734–44. [PubMed: 25020033]
32. Montero D, et al., Intracellular glutathione pools are heterogeneously concentrated. Redox Biol, 2013. 1: p. 508–13. [PubMed: 24251119]
33. Forman HJ, Zhang H, and Rinna A, Glutathione: overview of its protective roles, measurement, and biosynthesis. Mol Aspects Med, 2009. 30(1–2): p. 1–12. [PubMed: 18796312]

34. Hastings KT and Cresswell P, Disulfide Reduction in the Endocytic Pathway: Immunological Functions of Gamma-Interferon-Inducible Lysosomal Thiol Reductase. Antioxid. Redox Signaling, 2011. 15(3): p. 657–668.
35. Lushchak VI, Glutathione homeostasis and functions: potential targets for medical interventions. J Amino Acids, 2012. 2012: p. 736837.
36. Gray GD, Basu S, and Wickstrom E, Transformed and immortalized cellular uptake of oligodeoxynucleoside phosphorothioates, 3'-alkylamino oligodeoxynucleotides, 2'-O-methyl oligoribonucleotides, oligodeoxynucleoside methylphosphonates, and peptide nucleic acids. Biochem Pharmacol, 1997. 53(10): p. 1465–76. [PubMed: 9260874]
37. Cheng Y, et al., MicroRNA-145, a novel smooth muscle cell phenotypic marker and modulator, controls vascular neointimal lesion formation. Circ Res, 2009. 105(2): p. 158–66. [PubMed: 19542014]
38. Rong JX, et al., Transdifferentiation of mouse aortic smooth muscle cells to a macrophage-like state after cholesterol loading. Proc Natl Acad Sci U S A, 2003. 100(23): p. 13531–6. [PubMed: 14581613]
39. Shankman LS, et al., KLF4-dependent phenotypic modulation of smooth muscle cells has a key role in atherosclerotic plaque pathogenesis. Nat Med, 2015. 21(6): p. 628–37. [PubMed: 25985364]
40. Naghavi M, et al., From vulnerable plaque to vulnerable patient: a call for new definitions and risk assessment strategies: Part II. Circulation, 2003. 108(15): p. 1772–8. [PubMed: 14557340]
41. Virmani R, et al., Pathology of the vulnerable plaque. J Am Coll Cardiol, 2006. 47(8 Suppl): p. C13–8. [PubMed: 16631505]
42. Zhou Y, et al., Asperlin Inhibits LPS-Evoked Foam Cell Formation and Prevents Atherosclerosis in ApoE(−/−) Mice. Mar Drugs, 2017. 15(11).
43. Meir KS and Leitersdorf E, Atherosclerosis in the Apolipoprotein E–Deficient Mouse. Arteriosclerosis, Thrombosis, and Vascular Biology, 2004. 24(6): p. 1006–1014.
44. Lobatto ME, et al., Perspectives and opportunities for nanomedicine in the management of atherosclerosis. Nat Rev Drug Discov, 2011. 10(11): p. 835–52. [PubMed: 22015921]
45. Collaboration CMS, et al., Probing color coherence effects in pp collisions at [Formula: see text]. Eur Phys J C Part Fields, 2014. 74(6): p. 2901. [PubMed: 25814895]
46. Doran AC, Meller N, and McNamara CA, Role of smooth muscle cells in the initiation and early progression of atherosclerosis. Arterioscler Thromb Vasc Biol, 2008. 28(5): p. 812–9. [PubMed: 18276911]
47. Woollard KJ and Geissmann F, Monocytes in atherosclerosis: subsets and functions. Nat Rev Cardiol, 2010. 7(2): p. 77–86. [PubMed: 20065951]
48. O'Sullivan JF, Martin K, and Caplice NM, Microribonucleic acids for prevention of plaque rupture and in-stent restenosis: "a finger in the dam". J Am Coll Cardiol, 2011. 57(4): p. 383–9. [PubMed: 21251577]
49. Jacobsen K, et al., Diverse cellular architecture of atherosclerotic plaque derives from clonal expansion of a few medial SMCs. JCI Insight, 2017. 2(19).

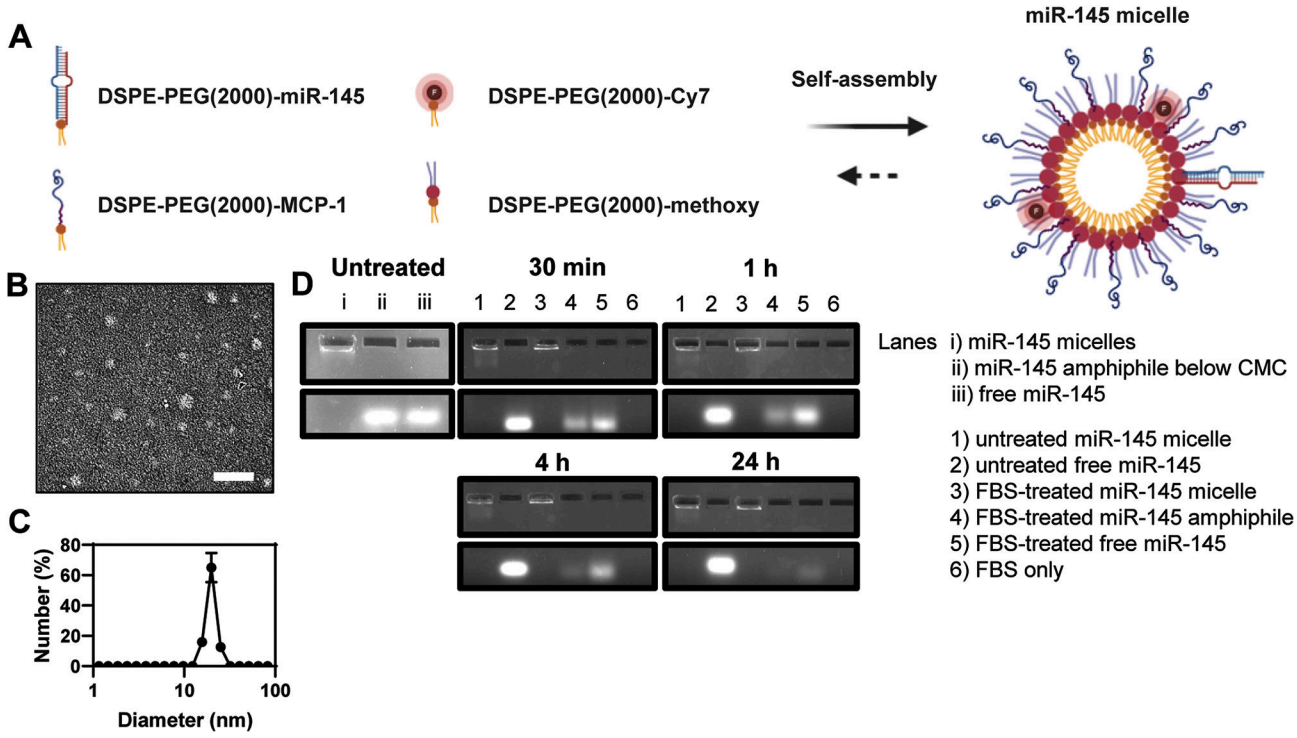

Fig. 1. Schematic and characterization of miR-145 micelles.

(A) Schematic of the self-assembly and multifunctionality of miR-145 micelles. (B) TEM images of miR-145 micelles. Scale bar = 200 nm. (C) DLS of miR-145 micelles. (D) Gel shift assays confirm miR-145 is protected when incorporated into micelles, nuclease degradation for up to 24 hours.

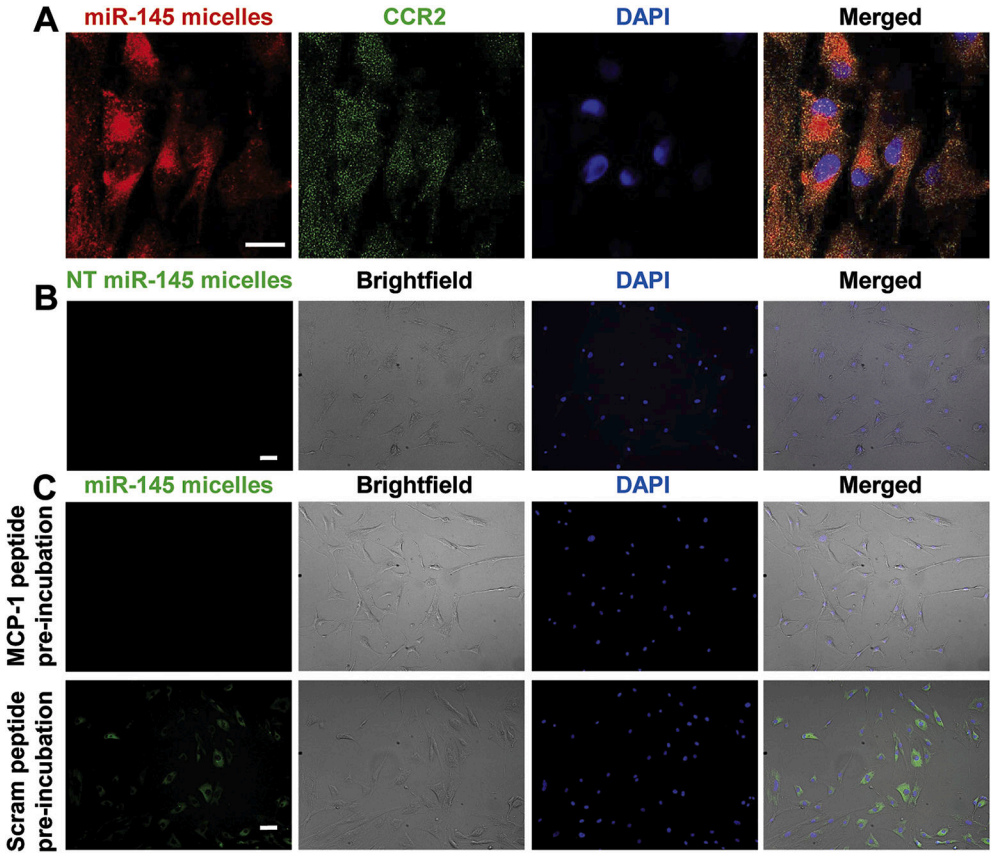

Fig. 2.

miR-145 micelle binding on VSMCs. (A) miR-145 micelles bind to CCR2 on VSMCs. Scale bar = 25 μm. (B) NT miR-145 micelles show no binding to diseased patient VSMCs. Scale bar = 100 μm. (C) Preincubation with MCP-1 significantly reduces miR-145 micelle binding, whereas preincubation with scrambled MCP-1 peptide does not affect miR-145 micelle binding to VSMCs. Scale bar = 100 μm.

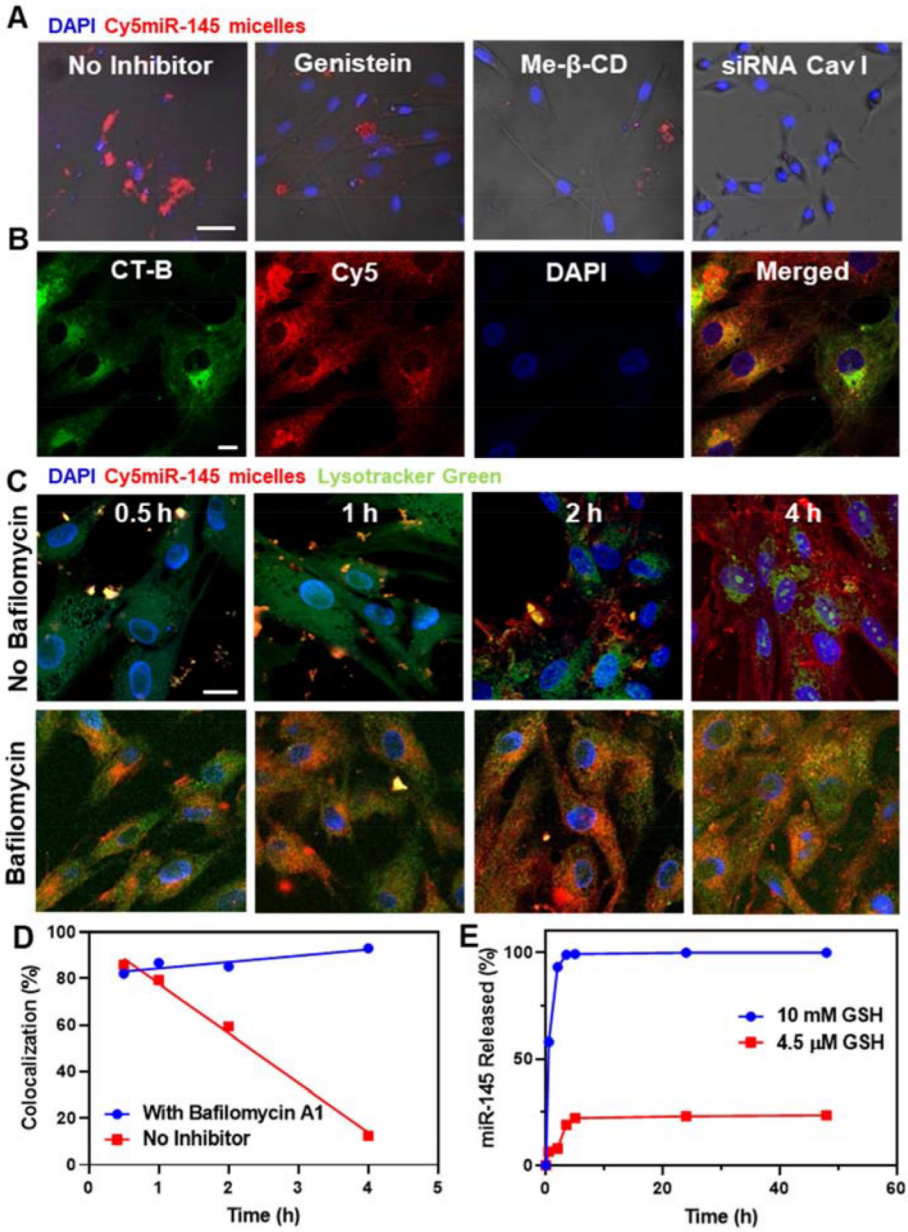

Fig. 3.

Cellular internalization, endosomal escape, and release of miR-145 micelles. (A) Fluorescence images of hASMCs incubated with Cy5miR-145 micelles (red) and endocytosis inhibitors. Scale bar = 50 μm. (B) hASMCs incubated with miR-145 micelles and treated with CT-B confirm micelle internalization is through caveolae-mediated endocytosis. Channels: Cy5-micelles (red) and CT-B (green). Scale bar = 20 μm. Time-dependent endosomal escape of Cy5miR-145 micelle in hASMCs (C) without and with bafilomycin A1. Nuclei were stained with DAPI (blue). Scale bar = 20 μm. (D) Percent colocalization of miR and endosomes. (E) Release profiles of miR-145 from micelles show release of miR-145 at intracellular GSH concentrations (10 mM).

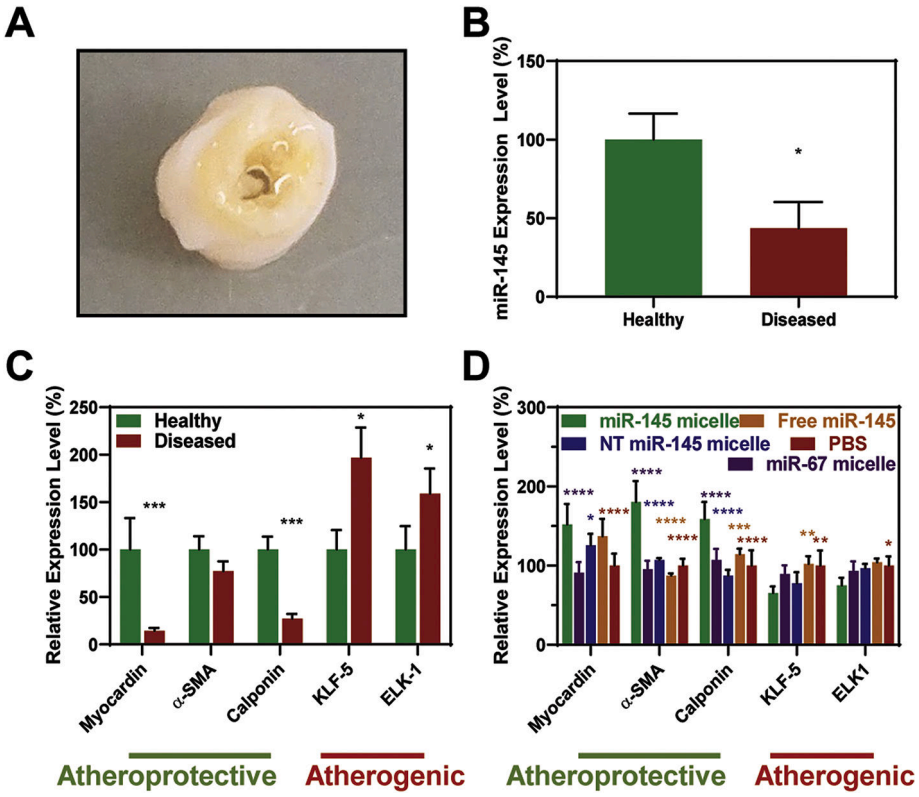

Fig. 4.

miR-145 micelles rescue VSMC contractile markers and silence synthetic markers. (A) Patient-derived, tibial artery samples with significant plaque build-up used to isolate VSMCs. These VSMCs have (B) lower miR-145 expression compared to VSMCs from healthy tissue (N = 3; *$p < 0.05$) and (C) lower endogenous expression of contractile markers and higher expression of synthetic markers (N = 4; *$p < 0.05$, ***$p < 0.001$ compared to healthy samples). (D) miR-145 micelle treatment on VSMCs derived from diseased arteries rescue contractile markers and downregulate synthetic markers (N = 4; *$p < 0.05$, ***$p < 0.001$, relative to miR-145 micelles).

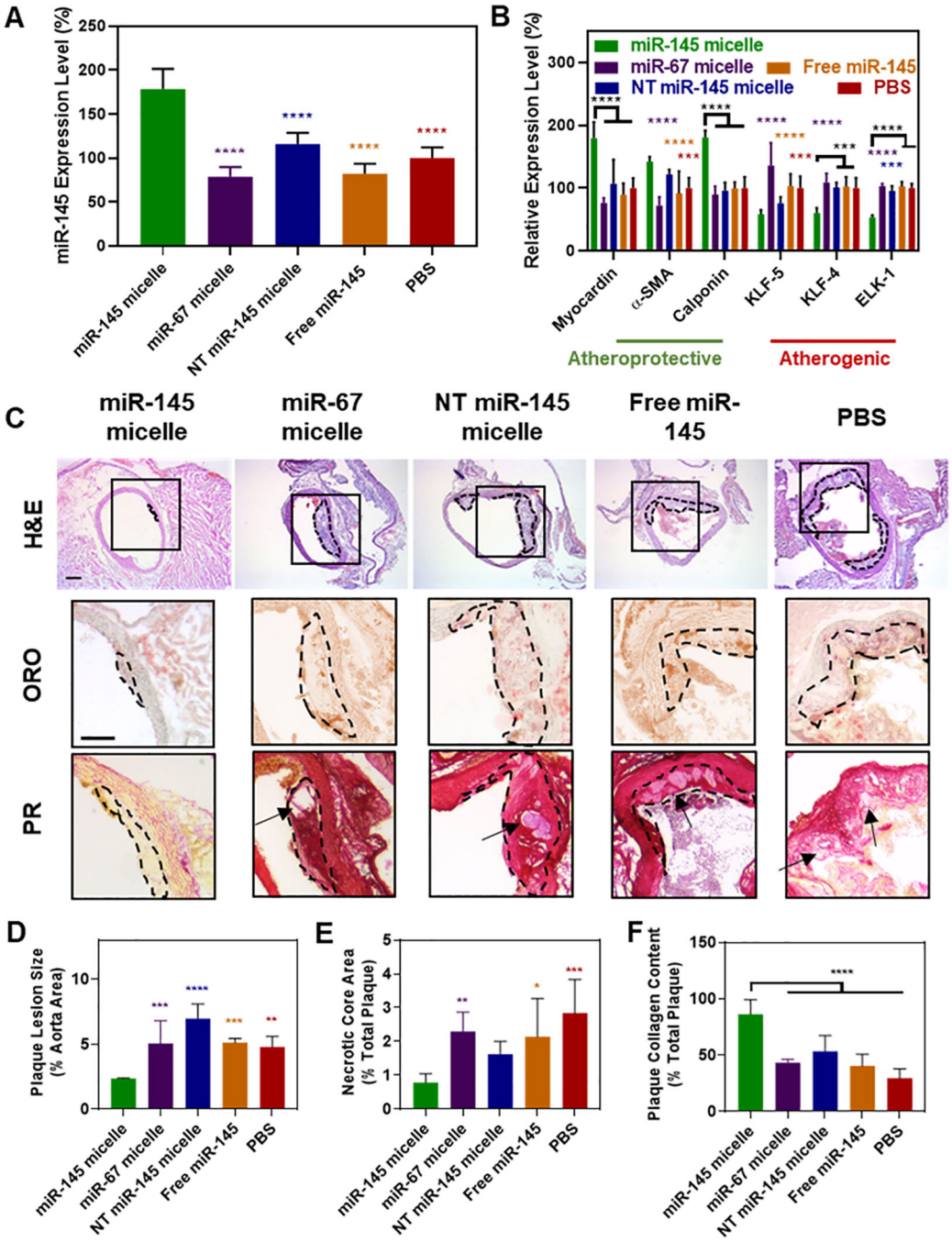

Fig. 5.

miR-145 micelles promote contractile VSMCs and prevent atherogenesis in early-stage disease. (A) miR-145 and (B) myocardin, α-SMA, calponin, KLF-5, KLF-4, and ELK-1 expression in VSMCs derived from early-stage atherosclerotic mice (N = 6). (C) Representative histological cross-sections of the ascending aorta stained with H&E, ORO, and PR (plaques: dotted black line, necrotic core: arrows). Scale bar = 200 μm. miR-145 micelle treatment decreases (D) plaque lesion size and (E) necrotic core area, while preserving (F) collagen content in plaques (Note: N = 6 for all treatment groups, except

miR-145 micelles with N = 4 as two mice did not form plaques, *p < 0.05, **p < 0.01, ***p < 0.001, ****p < 0.0001 compared to miR-145 micelles).

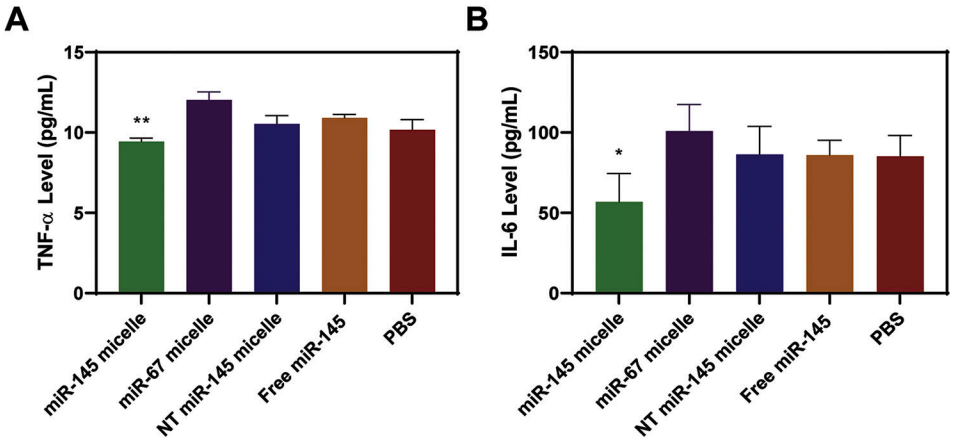

Fig. 6.

Anti-inflammatory effects of miR-145 micelles. Mice treated with miR-145 micelles show a decrease in serum (A) TNF-α and (B) IL-6 in early-stage ApoE$^{-/-}$ mice (N = 6; *$p < 0.05$, **$p < 0.01$).

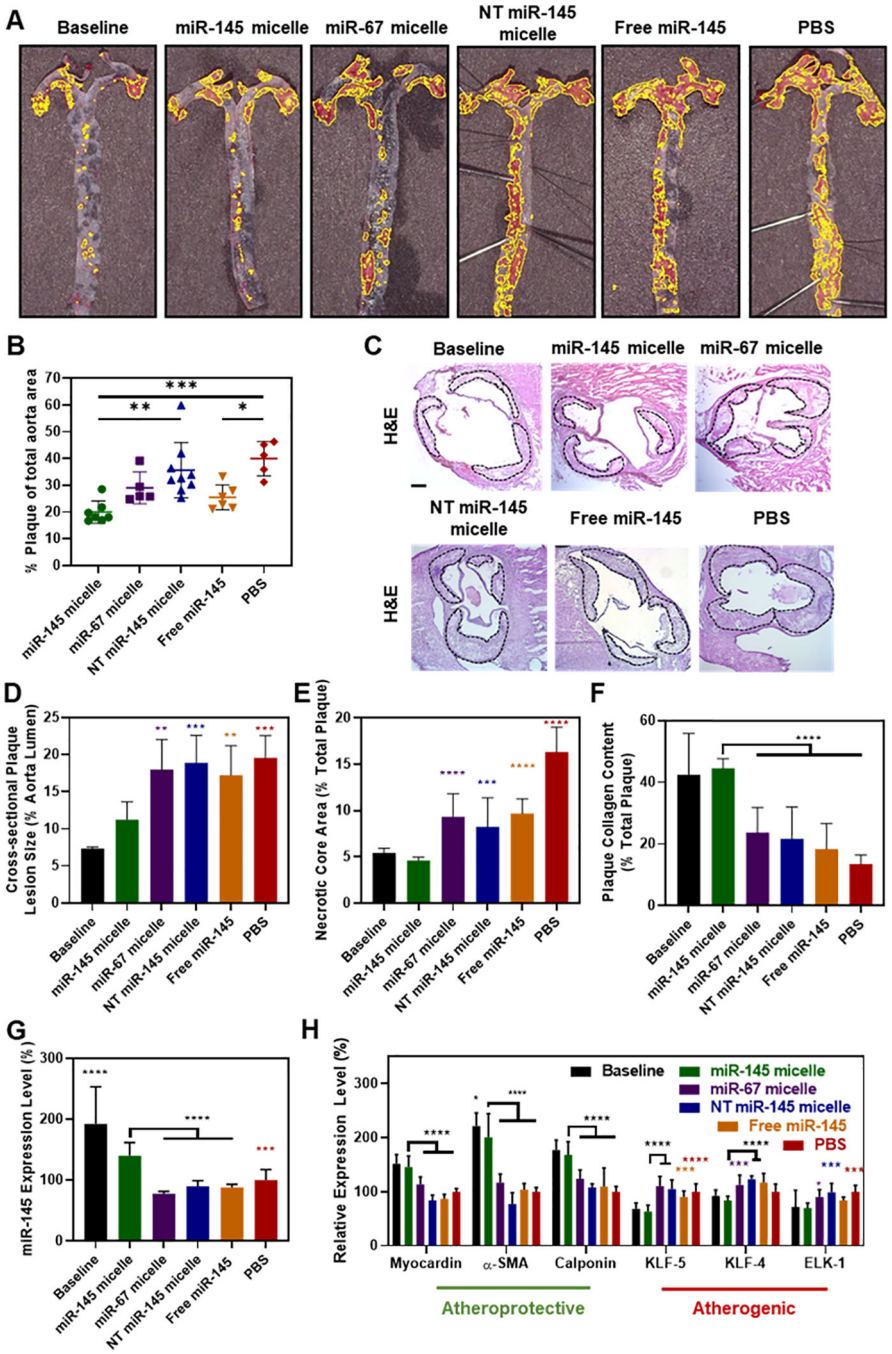

Fig. 7. miR-145 micelles promote contractile VSMCs and reduce plaque progression in mid-stage atherosclerotic mice.

(A) *En face* ORO stains of arteries show fewer plaques (yellow outline) in miR-145 micelle-treated mice and the baseline control (N > 5). (B) Quantification of ORO *en face* staining (N > 5). (C) Representative histological images of the aortic root stained with H&E showing plaques (dotted black line). Scale bar = 200 μm. Analysis of (D) cross-sectional plaque lesion size, (E) necrotic core area, and (F) collagen (N > 11 for treatment groups, N = 6 for baseline). (G) miR-145 expression and (H) mRNA expression of contractile and synthetic

phenotype markers in VSMCs from mid-stage atherosclerotic mice (N = 6; *p < 0.05, **p < 0.01, ***p < 0.001, ****p < 0.0001 compared to miR-145 micelles).

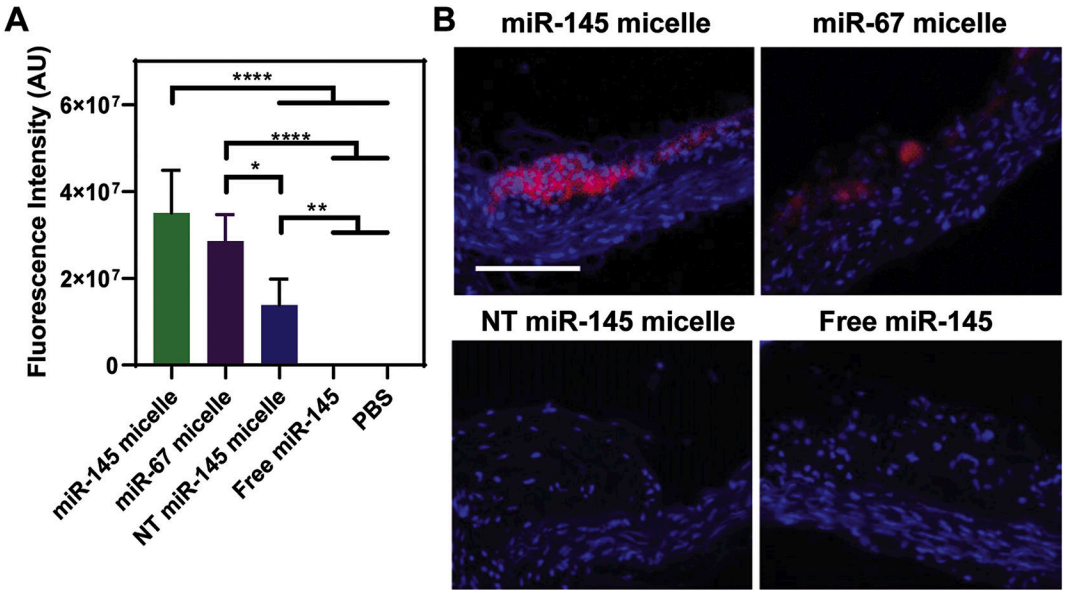

Fig. 8.

In vivo targeting of miR-145 micelles. (A) Fluorescence quantification in aortas of atherosclerotic mice show miR-145 micelles accumulate to the greatest degree compared to miR-67 micelles and NT miR-145 micelles (N = 6). (B) Histological analyses show miR-145 micelles (red) accumulate in plaques. Scale bar = 100 μm.

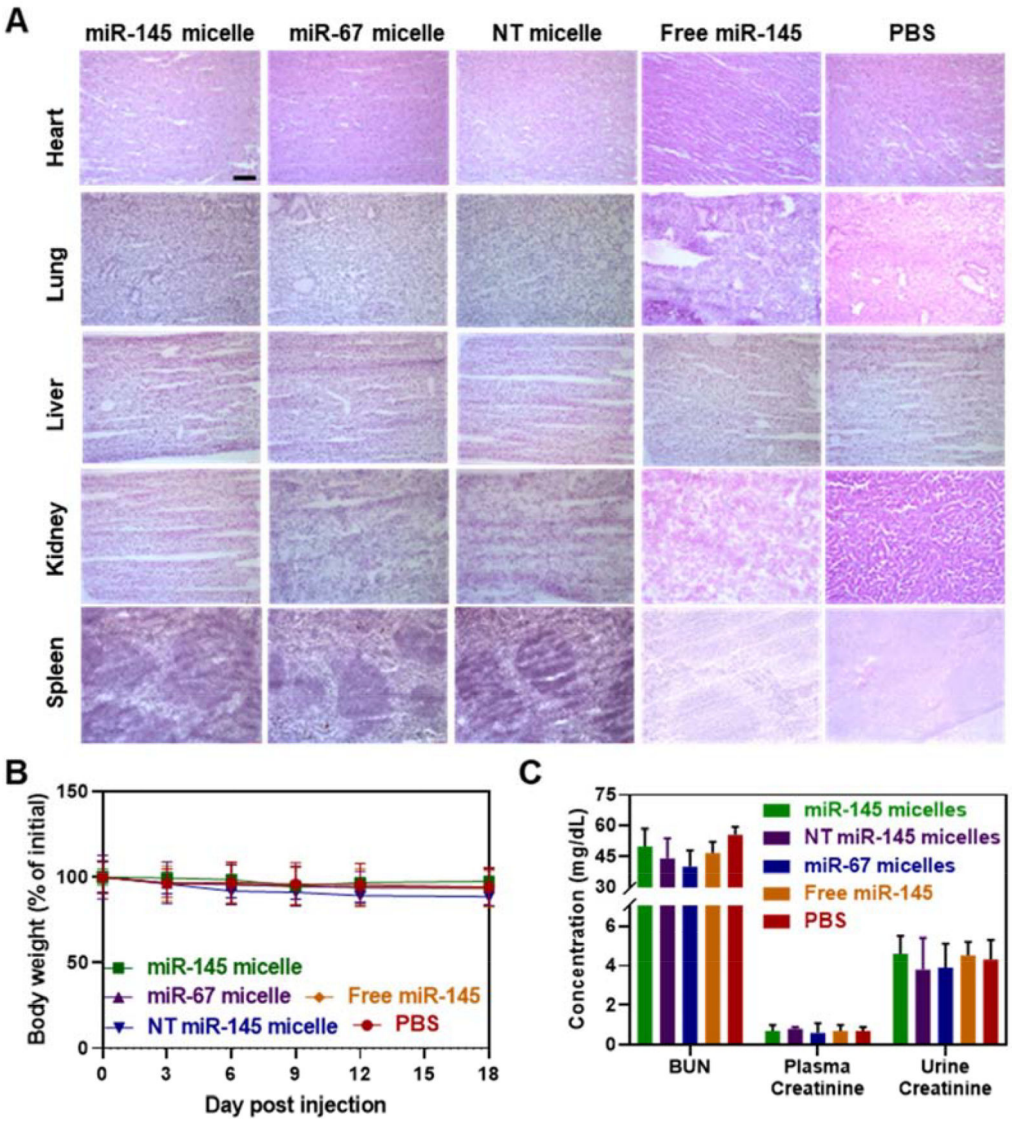

Fig. 9. ***In vivo*** **biocompatibility of miR-145 micelles.**

(A) H&E staining of major organs show no significant morphological changes associated with miR-145 micelles in mid-stage atherosclerotic mice (NT micelle = NT miR-145 micelle). Scale bar = 100 μm. (B) No significant change in body weight was observed for all groups, demonstrating the safety and tolerance of micelles (N = 12). (C) BUN and creatinine measurements confirm kidney health of mice and safety of micelles (N = 6).

Table 1

Size, polydispersity, and zeta potential of micelles.

	Diameter (nm)	PDI	Zeta Potential (mV)
miR-145 micelle	21.7 ± 2.2	0.21 ± 0.04	15.1 ± 0.2
MCP-1 micelle	14.6 ± 4.2	0.19 ± 0.09	13.6 ± 0.7
miR-67 micelle	21.5 ± 3.1	0.18 ± 0.08	11.8 ± 0.4
NT miR-145 micelle	23.3 ± 4.0	0.19 ± 0.08	8.06 ± 0.1